Research Square

Preprints are preliminary reports that have not undergone peer review.
They should not be considered conclusive, used to inform clinical practice,
or referenced by the media as validated information.

Monitoring the Effect of Urbanization on Atmospheric Thermodynamics over Bhubaneswar under Recent Climatic Conditions

Bhavana Thilakan
Amrita Vishwa Vidyapeetham
Jyotirmayee Satapathy
jyotirmayees@am.amrita.edu

Amrita Vishwa Vidyapeetham

Article

Keywords: Urbanization, Land Surface Temperature, Mann-Kendall trend test, INSAT 3D/3DR, ERA5 reanalysis, pre-convective instability, vertical wind shear, Bhubaneswar

Posted Date: August 19th, 2026

DOI: https://doi.org/10.21203/rs.3.rs-10471691/v1

License: This work is licensed under a Creative Commons Attribution 4.0 International License.
Read Full License

Additional Declarations: No competing interests reported.

Monitoring the Effect of Urbanization on Atmospheric Thermodynamics over Bhubaneswar under Recent Climatic Conditions.

Bhavana Thilakan, Jyotirmayee Satapathy*
Department of Physics, Amrita Vishwa Vidyapeetham, Amritapuri, India, 690525
*corresponding author email-id: jyotirmayees@am.amrita.edu

Abstract - The accelerating pace of urbanization is transforming the land-atmospheric interactions, resulting in alterations to the atmospheric thermodynamics that influence the local weather and climate. This study carries out an analysis over Bhubaneswar, India, combining 10 years (2015-2024) of satellite observations (INSAT 3DR) along with assimilation model, ERA5 land, pressure-level, and single-level reanalysis dataset. Daily data for Land Surface temperature (LST), surface energy fluxes, boundary-layer height, tropospheric moisture and thermodynamic variables, pre-convective instability indices, and vertical wind shear were tested for monotonic trends using the autocorrelation-corrected Hamed-Rao modified Mann-Kendall test with Theil-Sen slope estimation, stratified by season. Seasonal analyses were performed for the MAM (March-April-May) and ONDJF (October-November-December-January-February) seasons, whereas instability and wind-related variables were evaluated for MAM, JJAS (June-July-August-September), and ONDJF. Results show for pre-monsoon, MAM season, there is a statistically significant increase in LST over the years, accompanied by drying at 950 hPa, moistening aloft at 500 hPa, and a weakening of a 950-500 hPa vertical wind shear while in post-monsoon winter (ONDJF) surge in sensible heat flux ($p = 0.037$), a corresponding deepening of the boundary layer, near-surface drying, and increasing wind shear was observed. In the annual mean and annual 90th percentile-based assessment, the values of Total Totals Index shifted significantly in both MAM (decreasing, $p = 0.012$) and JJAS (increasing, $p = 0.032$) seasons. A deseasonalized correlation assessment highlights that the coupling between boundary layer height and near surface wind speed survives removal of the monsoon annual cycle, whereas most other raw correlations do not. Overall, this study provides robust evidence that rapid urbanization has altered the thermodynamic structure of the lower atmosphere, indicating an overall increase in instability over Bhubaneswar offering insights into urban climate processes and their implications for regional weather and climate under recent climatic conditions.

Index terms- Urbanization, Land Surface Temperature, Mann-Kendall trend test, INSAT 3D/3DR, ERA5 reanalysis, pre-convective instability, vertical wind shear, Bhubaneswar.

I. Introduction

The urban land-cover transformation constitutes one of the most intensive forms of anthropogenic land-atmospheric changes and has been extensively reported to influence the local energy partitioning, boundary-layer structure, and near-surface thermodynamics under diverse climatic settings [1-5]. Conversion of vegetated and moist surfaces with low albedo to impervious materials along with expanding traffic and industrial activities that introduces aerosols and combustion by-products eventually affects the local atmospheric composition and leads to an increase in the fraction of net radiation returning to the atmosphere as sensible rather than latent heat [5,6], thereby deepening the daytime planetary boundary layer, and affecting the vertical distribution of the moisture and static energy in the lower and middle troposphere [7,8]. Since these alterations operate on the same variables that governs the pre-convective instability [9], a parallel question of practical significance is whether such urbanization-induced thermodynamic changes coincide with any detectable shift in the atmospheric conditions associated with severe localized convective activities.

Urban modification not only affects the surface energy partitioning but also alters the local wind patterns and boundary-layer circulation, as increased surface roughness from building geometry disturbs the smooth airflow and induces the mechanical turbulence, channelized flow, and wake effects, while differential heating between the built-up areas and the surroundings promotes the thermally driven urban-rural circulation cells that interact with the prevailing synoptic flow [3,5,6]. These coupled dynamically-thermally produced changes will be transmitted to the planetary boundary layer, where they contribute to shifts in the convective triggering and organization [9] and to boundary-layer thermal responses influenced by horizontal advection [7].

Concurrently, the characteristics of urban centres like anthropogenic activities and lifestyle patterns perturb the composition of the near surface atmosphere, introducing aerosols, greenhouse gases, and anthropogenic heat generated from industries, transportation and the energy use that further alters the local radiative balance and

atmospheric stratification [1]. Collectively, these structural and compositional changes make urbanization a multifaceted modifier of the atmospheric environment, reshaping circulation patterns, wind fields, and thermodynamic conditions. Such changes have already been linked with measurable alterations in convective rainfall intensity across rapidly urbanizing tropical regions [1,8] providing a strong rationale for examining whether similar modifications extend to the specific environment governing severe local convection.

Bhubaneswar, the capital city of Odisha, India, has undergone a widespread built-up area growth over the past decades [10-13] and recorded a greater occurrence of extreme weather events-including high intensity heat waves, sporadic pre-monsoon convective storms, and heavy rainfall episodes-highlighting the need to determine whether the regions rapid urbanization is modifying the local atmospheric environment beyond the natural variability. Prior studies have approached this question from multiple perspectives: land surface temperature together with land-use changes have demonstrated the growth of urban heat signature concurrent with the accompanying urban expansion [10,11], while others have reported how the city's asymmetric topography affects the winter surface temperature patterns in an urban settings [12]. Most recent works have contextualized Bhubaneswar follows the broader pattern of urbanization-associated regional warming observed across Indian cities [13]. However, many local-scale assessments are based on single variable data stream (e.g. LST) rather than integrating thermodynamic and convective instability conditions all together, thereby limiting their capacity to establish the physical mechanisms connecting surface warming to atmospheric responses. Thus, it leaves open the question of whether a physically coherent, multi-level signature of urbanization-extending from the surface energy budget to the free-tropospheric thermodynamics and shear environment-can be resolved using longer and more comprehensive dataset which is systematically examined.

The present work addresses this gap by collecting a decade long (2015-2024) multi-instrument, multi-level dataset over Bhubaneshwar and systematically analysing, whether a consistent set of urbanization-led trends is present across the surface energy budget, boundary-layer depth, tropospheric moisture and thermodynamic structure, pre-convective instability indices, and vertical wind shear.

The investigation addresses three primary research objectives. First, it characterizes for the last decade, season-stratified trends in land surface temperature together with a suite of independent urbanization-sensitive thermodynamic proxies. Second, it examines whether the seasonal-mean and upper-tail characteristics of established pre-convective indices such as Convective Atmospheric Potential Energy (CAPE), Convective Inhibition (CIN), K-Index (KI), Total Total Index (TTI) and Lifted Index (LI) shifted over the study period. Finally, the study evaluates, using lag-lead cross-correlation and a deseasonalization control, whether wind-field variability provides physically consistent supporting evidence. The manuscript is organized as follows. Section II describing the study area and the five corresponding datasets. Section III details the statistical methodology. Section IV represents the analytical results. Section V discusses the physical interpretations of the study, and section VI concludes.

II. Study Area and Data

A. Study Area and Period

The study is centred on Bhubaneswar, India (20.2726°N, 85.8331° E), for a period of ten-years (2015-2024). To minimize the influence of the pronounced seasonal variability associated with the Indian monsoon system, all analyses were stratified into three seasons: pre-monsoon (MAM: March-May). monsoon (JJAS: June-September), and post-monsoon-winter (ONDJF: October-February, spanning the calendar-year boundary)

B. Data Sources

Five independent datasets were brought together, as outlined in Table I. Land Surface temperature (LST) was sourced from the INSAT-3D Imager (2015-2023) and INSAT 3DR Imager (2024), which was pre-processed as a 3x3-pixel spatial mean centred on Bhubaneswar at half-hourly resolution [14]. Vertical thermodynamic profile variables were sourced from INSAT-3D Sounder (2015-2016) and INSAT-3DR Sounder (2017-2024) at the nearest grid pixel [14]. Equivalent Potential Temperature (θe) [15], Moist Static Energy (MSE) [16,17], Atmospheric Energy (AE) [18] were derived using certain sounder-variables. Surface turbulent heat fluxes (sensible and latent) were collected from ERA5-Land at 0.1° x 0.1° resolution [19]. Pressure level variables-

Relative humidity, specific humidity, vertical velocity, divergence, relative vorticity, and the zonal and meridional wind components were obtained from ERA5 at 950,750, and 500 hPa levels [20] via bilinear interpolation to the study coordinates. Single level convective and boundary-layer variables (Convective Available Potential Energy (CAPE), Cloud Base Height (CBH), Convective Inhibition (CIN), dew point temperature at 2 m, the K-Index, and Planetary Boundary Layer Height (PBLH)) were obtained from ERA5 single level [20] with same interpolation technique for the study location.

TABLE I. Data Sources used in this study.

Source	Variables	Resolution	Period
INSAT-3D/3DR Imager	Land Surface Temperature (LST)	3x3 pixel spatial mean, 30 min	2015-2024
INSAT-3D/3DR Sounder	Air Temperature, Water Vapor Mass Mixing Ratio, Geopotential Height, LI, Total Precipitable Water (950/750/500 hPa)	Nearest pixel	2015-2024
Derived Sounder variables	θe, MSE, AE	Nearest pixel	2015-2024
ERA5-Land	Sensible and Latent heat flux	0.1°x 0.1°, hourly	2015-2024
ERA5 Pressure levels	RH, SH, VV, Divergence, RV, U and V components of wind (950/750/500 hPa)	Bilinear Interpolated	2015-2024
ERA5 single levels	CAPE, CBH, CIN, D2M, KI, PBLH	Bilinear Interpolated	2015-2024

C. Preprocessing and Data Merging

Each dataset underwent variable-specific quality control using the physically defined bounds according to the respective providers prior to aggregation. According to the characteristics of the core scientific studies conducted here, two temporal extraction windows were selected: A noon window, used for the primary urbanization-trend and dynamical evidence and an afternoon window (13:30 – 18:30 IST), used for the pre-convective instability analyse because severe convective initiation over the study area is climatologically most probable in this period [21]. Within each window, sub-daily observation was compressed to a daily mean. The five daily series datasets after independent processing were then combined using an inner join method based on date, filtering the dataset to retain only fully collocated records.

III. Methodology

A. Trend Detection

Monotonic trends in each daily seasonal time series were evaluated using the modified Hamed-Rao Mann-Kendall test, which incorporates a variance correction to account for serial autocorrelation associated to computing significance [22]. The daily geophysical time series are strongly autocorrelated, and the original Mann-Kendall test would mis-inflate the significance. Trend magnitudes were estimated using the Theil-Sen Slope estimator, a non-parametric estimator robust to outliers [23,24]. Statistical significance was evaluated at a two-sided significance level of $\alpha = 0.05$. Trend with $p<0.05$ were considered significant and the corresponding rate of change was estimated using the Theil-Sen slope estimator. Time series with $p \geq 0.05$ were classified as exhibiting no significant trend. The direction and strength of monotonic trends were characterized using Kendall's τ from the Hamed-Rao modified MK test. Kendall's τ varies between -1 and $+1$, with the sign indicating trend direction and the absolute value reflecting trend strength [24]. The corresponding rate of change was estimated using the Theil–Sen slope in the original units of each variable. Annual anomaly plots were generated with a baseline period of 2015-2019 to analyse the change of variables over the years.

B. Derived Thermodynamic Quantities

In addition to the retrieved variables, several quantities were derived to serve as urbanization-sensitive thermodynamic proxies: Equivalent potential temperature (θe) and moist static energy (MSE) at 950, 750,500 hPa and a column-integrated atmospheric Energy (AE) term [18], defined as in equation (1).

(1)

which is integrated in pressure coordinates over all 40 available sounder pressure levels.

C. Pre-Convective Instability Indices

Five conventional instability indices-Convective Available Potential Energy (CAPE), Convective Inhibition (CIN), the K-Index (KI) the Total Totals Index (TTI), and the Lifted Index (LI)-were assessed using the afternoon-window extraction. For each index and seasons, trends in the annual mean and annual 90^{th} percentile values were assessed using the modified Hamed-Rao MK test and Theil-Sen slope estimator. The annual mean reflects the long-term changes in the seasonal baseline for thermodynamic environment, while the 90^{th} percentile represents changes in high-end instability conditions associated with enhanced convective potential [25].

To provide a complementary perspective, seasonal observations were grouped into an early (2015-2019) and a recent (2020-20024) period. Gaussian distributions were then fitted separately to each period, and the final density curves were overlaid for each season to evaluate distributional shifts toward more extreme atmospheric conditions [26,27,28]. The resulted annual probability density functions quantitatively evaluate the temporal shifts in the distributions, with particular emphasis on changes in the tail characteristics, thereby highlighting progressive shifts toward conditions that are more favourable for severe convection.

D. Wind Shear as a Trend-Testable Dynamical Quantity

The Raw wind components and wind speed at an individual grid point are strongly influenced by transient, advective and synoptic-scale processes, and a Mann-Kendall trend applied directly to such series has limited interpretability. Therefore, Vertical Wind Shear (VWS), defined as the vector difference between the winds at 950 and 500 hPa [29], was used as a more robust diagnostic by reducing the influence of shared synoptic-scale variability between the two levels [30]. The magnitude of the VWS has thus been trend-tested in the same manner as thermodynamic variable described above, in addition to a simpler scale wind-speed-difference variant reported for comparison. The wind rose plot helps in demonstrating whether the wind directions and their frequencies changed over period.

E. Correlation, Lag-Lead and Deseasonalization Analysis

To understand whether the thermodynamic and dynamical fields co-vary in a way consistent with the hypothesized surface-heating-to-circulation pathway, the daily noon-window series resampled to weekly means and a correlation matrix was calculated between thermodynamic drivers (LST, sensible and latent heat flux, PBLH) and 950 hPa dynamical responses (wind speed, divergence, relative vorticity, vertical velocity), Temporal relationships were investigated via lag-lead cross-correlation, with a positive lag 0 inferred as the driver leading the response [31,32]. Since the Indian monsoon annual cycle can induce strong raw correlation between variable for reasons unrelated to any urbanization mechanism, deseasonalization control was additionally executed [33]: the mean seasonal cycle was removed from each weekly series prior to recomputing the correlation, and the percentage of raw correlation surviving this removal was taken to distinguish relationships that might be driven by seasonality alone from those with an independent interannual association.

IV. Results

A. Evidence of Surface and Boundary-Layer Change

LST exhibited a statistically significant increasing trend in the pre-monsoon season (MAM: $p<0.001$), in contrast no significant LST trend was observed in ONDJF ($p=0.586$) over the same study period. Figure I summarizes the significant ($p<0.05$) urbanization-proxy trends estimated using Mann-Kandall analysis in each season.

Same analysis in terms of time series plots of the trend significance with Theil-Sen trend line in shown in figure II. In MAM, the LST increase co-occurred with a significant decrease in Relative Humidity at 950 hPa ($p=0.008$), an increase in Relative Humidity and Specific Humidity at 500 hPa ($p=0.038$ and $p=0.031$, respectively), decrease in 750 hPa Geopotential Height ($p=0.016$), a decrease in 500 hPa Vertical Velocity ($p=0.008$, i.e. a shift towards stronger upward motion), and a decrease in 950-500 hPa Vector Wind Shear ($p <0.001$). Whereas in case of ONDJF, no significant LST trend was found, but ERA5-Land Sensible Heat Flux increased significantly ($p=0.037$), followed by a significant increase in PBLH ($p=0.020$), a decrease in 2m dewpoint temperature ($p=0.002$), a decrease in Specific Humidity at 950 hPa ($p <0.001$), a decrease in 950 hPa Water-Vapour Mass Mixing Ratio ($p=0.044$), a decrease in the column Atmospheric Energy ($p=0.004$), and an increase in 950-500 hPa vector wind shear ($p=0.015$). Annual anomaly plot for LST and Vertical velocity at 950 hPa shows an increasing trend while surface air temperature at 950 hPa shows a decline as seen in figure III. From these results we conclude that summer season for a urban climate facilitates low-level convection and convergence compared to winter season.

B. Pre-convective Instability Environment

Figure IV illustrates the monthly climatology of the weekly aggregated pre-convective instability indices (CAPE, CIN, KI, TTI and LI) for the study period. These indices are important to understand the thermodynamical inclinations over an urban climate. The 10 year-climatology reveals a distinct seasonal progression transitioning from comparatively stable conditions in ONDJF to enhanced atmospheric instability during MAM and JJAS. The seasonal evolution is marked by enhanced CAPE and TTI, increasingly negative LI values, and reduced convective inhibition, reflecting thermodynamic surroundings that becomes progressively more supportive of deep convection during warmer months.

Trend analyses of the annual average and annual 90th-percentile values are tabulated in table II which suggest that the extensive seasonal instability environment stayed generally stable during the study period. The K-Index revealed no significant statistical trends in either metric during any season. In contrast, CAPE showed a notable decrease during ONDJF, reflected in both the annual mean ($p = 0.020$) and the annual 90th percentile ($p = 0.012$), indicating a deterioration of both the dominant and elevated instability during the post-monsoon–winter period. The Total Totals Index displayed no notable alterations in its seasonal average; however, its upper-tail behaviour fluctuated seasonally, showing a significant drop in the 90th percentile during MAM ($p = 0.012$) and a significant rise during JJAS ($p = 0.032$), whereas no significant change was observed during ONDJF.

In addition to the trend analysis, Gaussian probability density functions were analysed for each season to evaluate distributional shifts toward more extreme atmospheric conditions and are presented in figure V. Comparisons between the early (2015–2017) and late (2022–2024) periods offer a more distinct representation of long-term distributional shifts. Special focus was placed on the distribution tails as shifts in these areas indicate variations in the occurrence of environments linked to increased convective potential. In multiple instances, the distribution tails changed even with minimal or no alteration in the seasonal average, suggesting that shifts in extreme thermodynamic conditions might not be entirely reflected by statistics based solely on the mean of the data.

Overall, these findings indicate that the average seasonal thermodynamic conditions saw only slight variations from 2015 to 2024, whereas certain instability indices displayed season-specific alterations in their extreme-value traits. Thus, incorporating annual mean, annual 90th-percentile, and distributional analyses offers a more comprehensive evaluation of temporal variability in pre-convective atmospheric instability and its effects on conditions conducive to severe convection. Previously, it has been found that there is increasing convective activity and cumulous clouds in pre-monsoon season for this decade over Indian atmosphere [34].

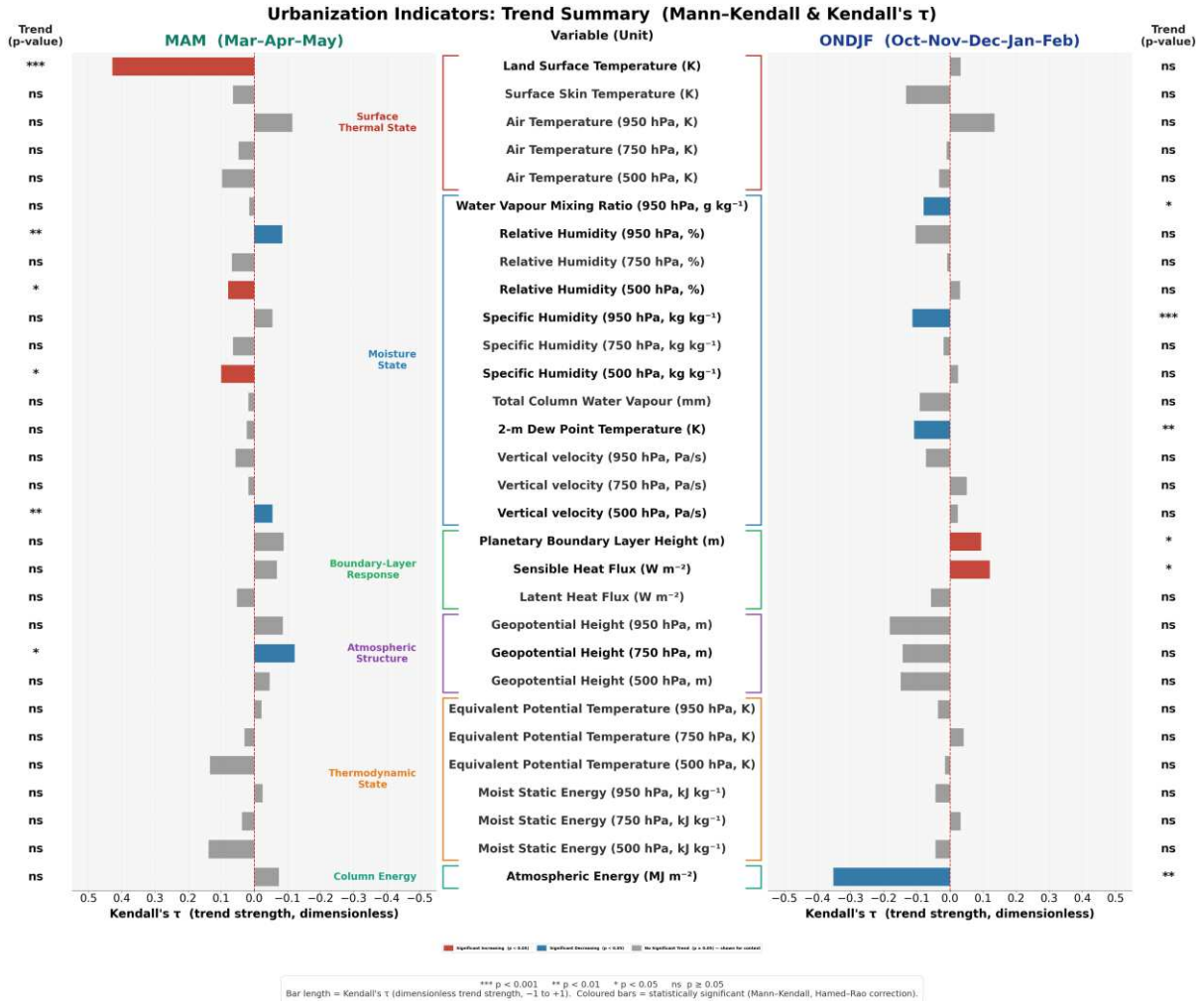


Figure I:Seasonal trend in urbanization-proxy variables (based on Kendall's τ values)

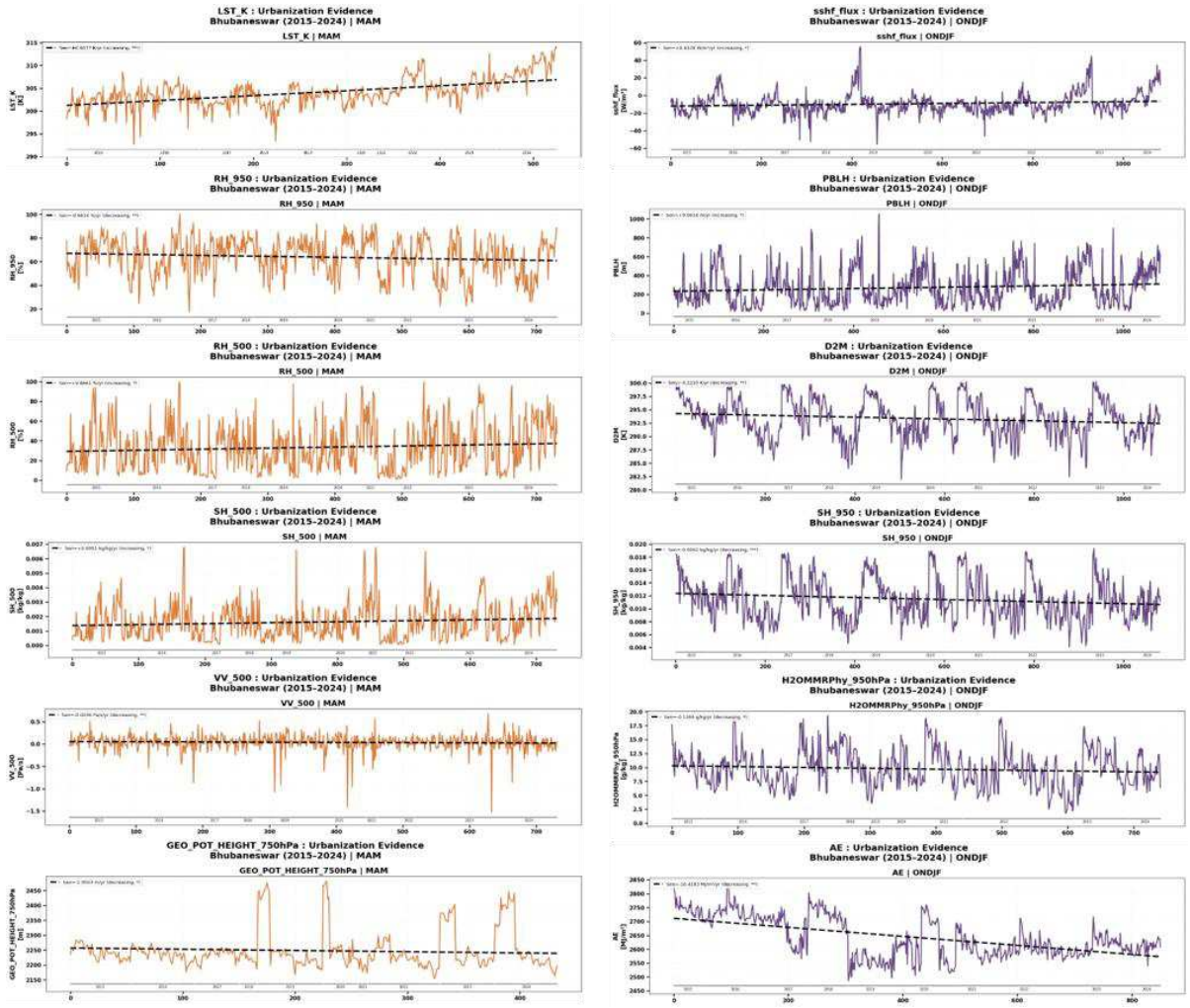


Figure II. Time series plots of the trend significance showing variables with Theil-Sen trend line.

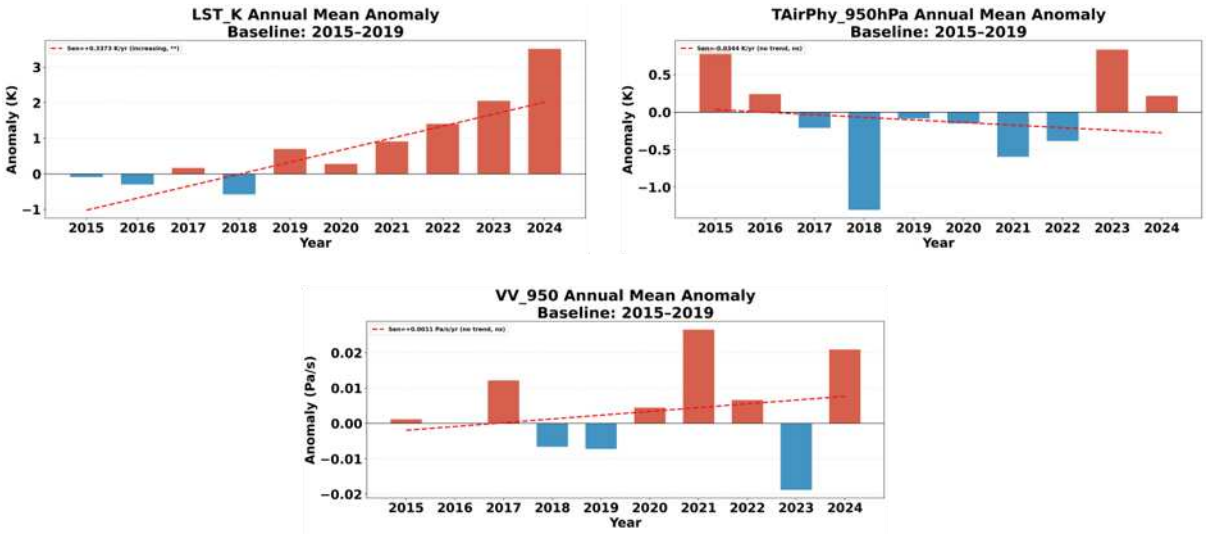


Figure III. Annual mean anomaly plots of LST, Air temperature at 950 hPa and Vertical Velocity at 950 hPa



Figure IV. The monthly climatology of the weekly aggregated pre-convective instability indices

TABLE II. Continuous-Value Trend Results for CAPE, KI, and TTI (Selected significant results)

Variable	Statistic	Season	Trend	p-value
CAPE	Mean	ONDJF	Decreasing	0.020
CAPE	90^{th} pct.	ONDJF	Decreasing	0.012
TTI	90^{th} pct.	MAM	Decreasing	0.012
TTI	90^{th} pct.	JJAS	Increasing	0.032

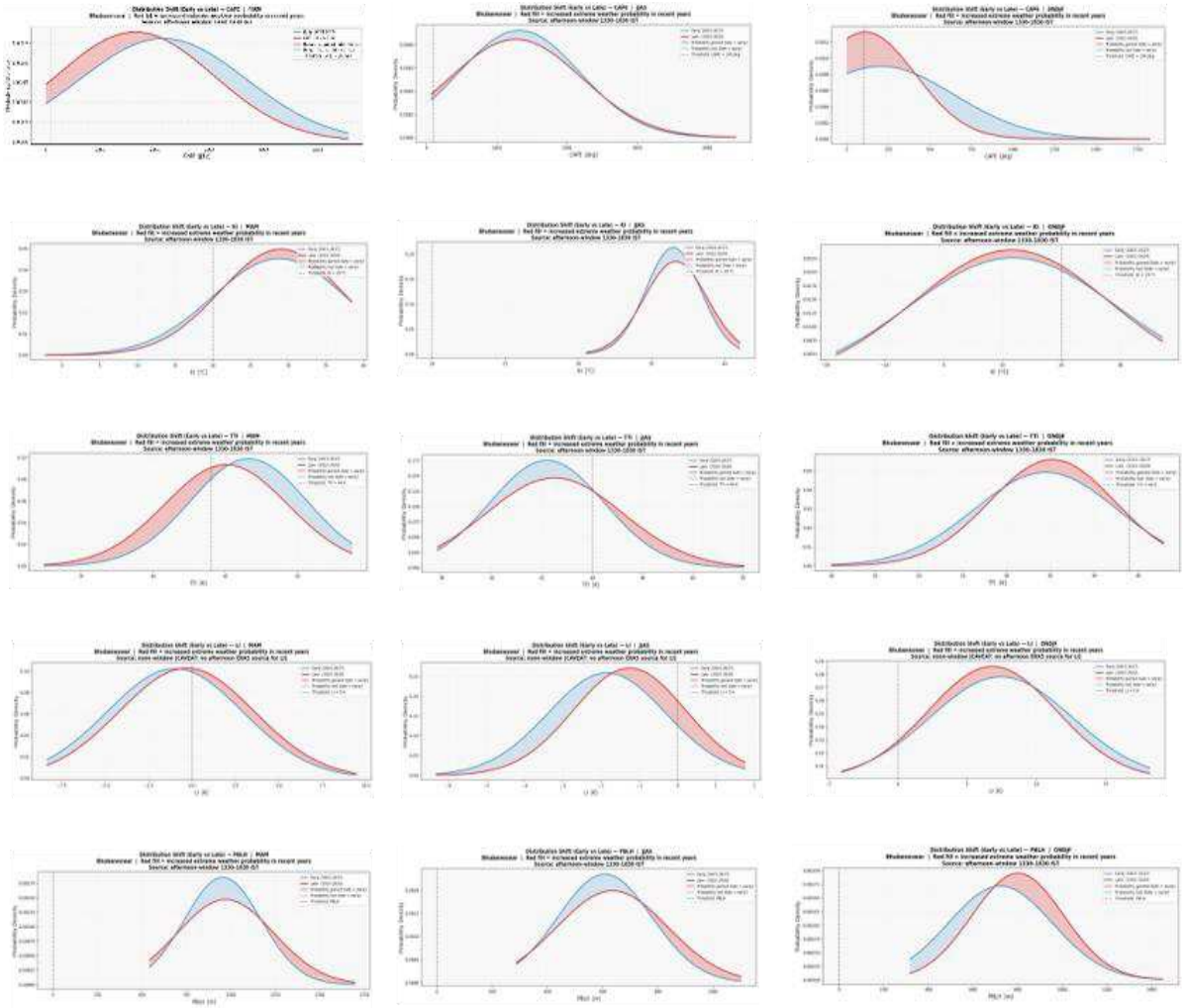


Figure V. Gaussian probability density functions demonstrating the comparison between the early (2015–2017) and late (2022–2024) periods for each season.

C. Dynamical corroboration

The wind-rose plot in figure VI indicates that the dominant wind directions and their frequencies remained largely unchanged between 2015–2019 and 2020–2024 across the 950, 750, and 500 hPa levels, suggesting that urbanization has had little influence on the prevailing atmospheric circulation over Bhubaneswar.

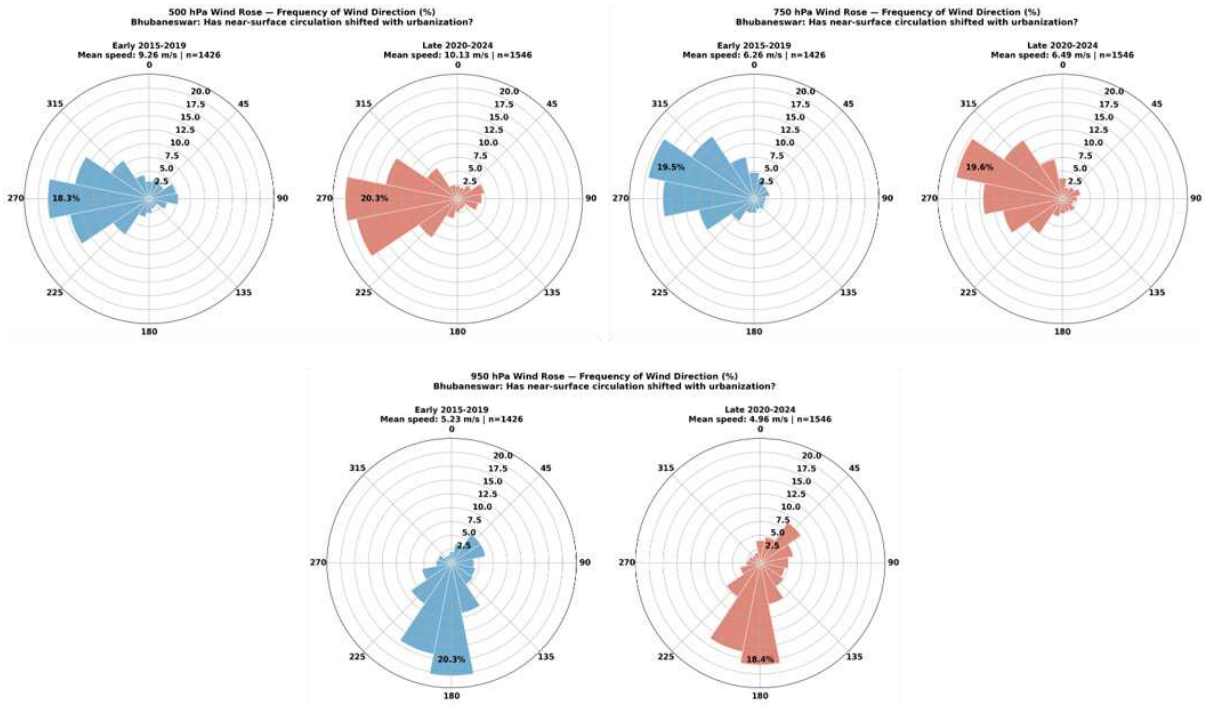


FIGURE VI. Early-(2015-2019) versus late-period (2020-2024) wind rose at 950 hPa

Vertical wind shear (950-500 hPa) expressed opposite-signed trends in MAM (decreasing, $p<0.001$) and OND JF (increasing, $p=0.015$), which is observed to be consistent with the season-dependent thermodynamic changes discussed in section IV-A. Lag-lead cross-correlation on the weekly-resampled data shown in figure VII, found three driver-response pairs in the potential thermodynamic driver led the corresponding dynamical response at a positive lag with a prominent peak correlation. The correlation rsults are presented in table III. From the results, it shows that sensible heat flux leading PBLH by one week (peak $r=0.688$), 950 hPa air temperature leading 950 hPa relative y two weeks (peak $r=0.614$), and sensible heat flux leading 950 hPa relative vorticities by six weeks (peak $r=0.574$).

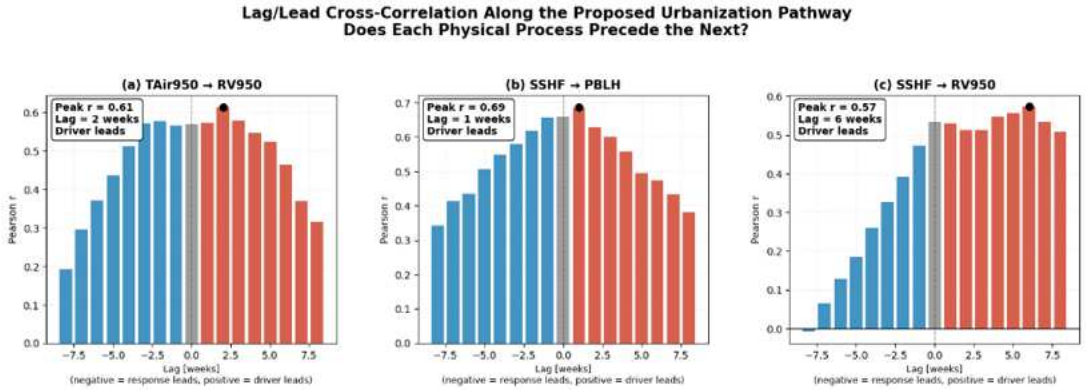


FIGURE VII. Lag-Lead Cross-Correlation Results.

TABLE III. Lag-Lead Cross-Correlation Results.

Driver	Response	Peak r	Lag (weeks)	n
950 hPa air temperature	950 hPa relative vorticities	0.614	2	326
Sensible heat flux	PBLH	0.688	1	443
Sensible heat flux	950 hPa relative vorticities	0.574	6	424

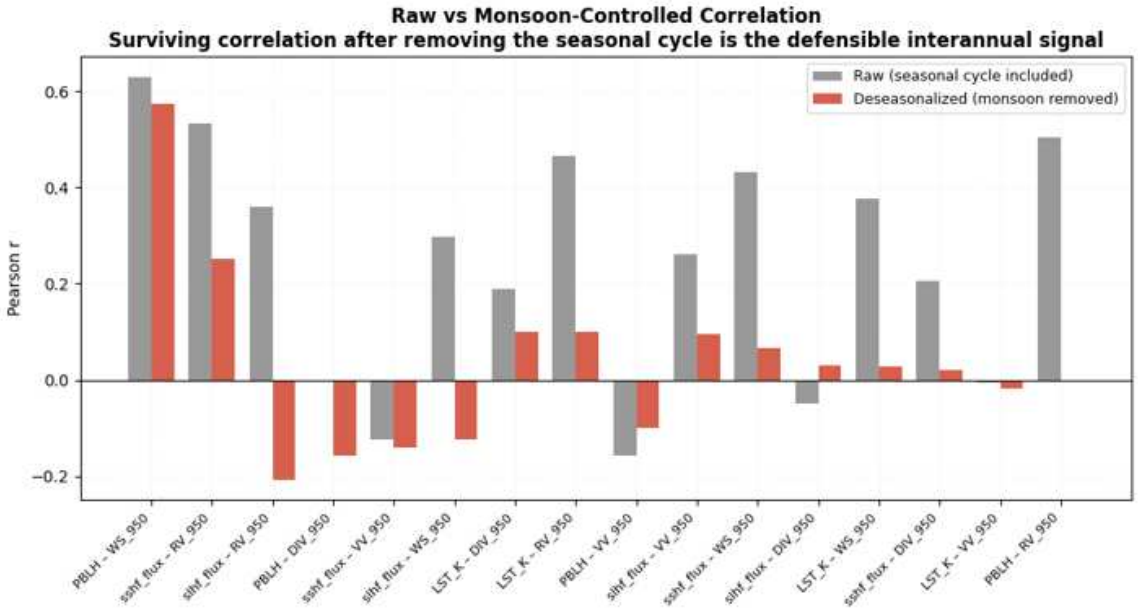


FIGURE VIII. Raw versus deseasonalized correlation coefficients for thermodynamic-dynamical variables pairs

The deseasonalization analysis of these parameteres are tabulted in table IV, shows that most raw correlations between thermodynamic and dynamical fields were substantially attenuated after removing the mean seasonal evolution. Figure VIII indicates that the parameters were largely governed by the common annual (monsoon) cycle rather than by persistent interannual relationship. The connecting link between PBLH and 950 hPa wind speed was the most robust retaining 90.9% of its raw correlation ($r_{raw} = 0.631$, $r_{deseasonalized}=0.574$, $p<0.001$) after deseasonalization in comparison, the correlation between sensible heat flux and 950 hPa relative vorticity retained a moderate fraction (47.2%) of its initial strength, wheels the association between sensible heat flux and 950 hPa divergence remained statistically significant but preserved a smaller proportion of the original correlation (9.8-61.1% across related pairing)

TABLE IV. Deseasonalized Correlation Survival (Selected Pairs)

Thermodynamic variables	Wind variables	r (raw)	r (deseasonalized)	% surviving
PBLH	WS, 950 hPa	0.631	0.574	90.9
Sensible heat flux	RV, 950 hPa	0.534	0.252	47.2
Latent heat flux	RV, 950 hPa	0.361	-0.208	57.6
Sensible heat flux	DIV, 950 hPa	0.207	0.020	9.8

V. Discussion

The findings presented in Section IV reveals a physically coherent, season-dependent chain of change i.e. during the pre-monsoon, a significant increase in land surface temperature is accompanied with lower-tropospheric drying, mid-tropospheric moistening, reduced deep-layer geopotential thickness, intensified upward motion, and a weaker deep-layer vertical wind shear, collectively indicating conditions that become progressively more favourable for convection. In contrast, the post-monsoon winter s associated with enhanced sensible heat flux a deeper planetary boundary layer, reduced near-surface moisture, declining column atmospheric energy, and strengthened vertical wind shear.

The lag-lead and deseasonalization correlation analysis further reinforce the physical consistency of those observations. Removal of the climatological seasonal cycle substantially reduced most thermodynamic-dynamical correlations, indicating that they primarily reflected seasonal variability. The persistent coupling between PBLH

and 950 hPa wind speed, however, remained evident suggesting a genuine interannual linkage consistent with boundary-layer mixing processes that transport higher-momentum air toward the surface.

Taken together, the thermodynamic and dynamical evidence indicates that atmospheric changes during the study period are strongly season dependent rather than uniformly expressed throughout the year. The observed changes suggest that season-dependent modifications in the large-scale atmospheric environment affects the convective potential through different physical processes during the pre-monsoon and post-monsoon-winter periods. While the findings should be interpreted considering the temporal coverage and spatial resolution of the available datasets, they provide a physically consistent perspective on recent environmental changer over the study region. A schematic summary of the seasonal thermodynamic evolution over Bhubaneswar (MAM and ONDJF) for the chosen study period, is shown in figure IX.

VI. Conclusion

A seasonally resolved, multi-dataset assessment of atmospheric thermodynamics over Bhubaneswar for the period 2015-2024 revealed distinct patterns of environmental change. A statistically significant pre-monsoon increase in land surface temperature and a significant post-monsoon-winter increase in sensible heat flux were each associated with coherent changes in PBLH, tropospheric moisture, and a deep-layer vertical wind shear while the mean instability environment exhibited little long-term change significant shifts in the upper-tail behaviour of the TTI highlighted season-dependent changes in environments favourable for convection. Furthermore, the persistence of the relationship between boundary-layer height and near surface wind speed following deseasonalization suggests that this coupling extends beyond the influence of the climatological annual monsoon cycle. Collectively, the findings indicate that change in thermodynamic conditions is consistent with urbanization-related atmospheric modification over Bhubaneshwar. Future studies should examine whether the observed thermodynamic and dynamical changes are reflected in long-term trends in the frequency and intensity of observed severe convective events.

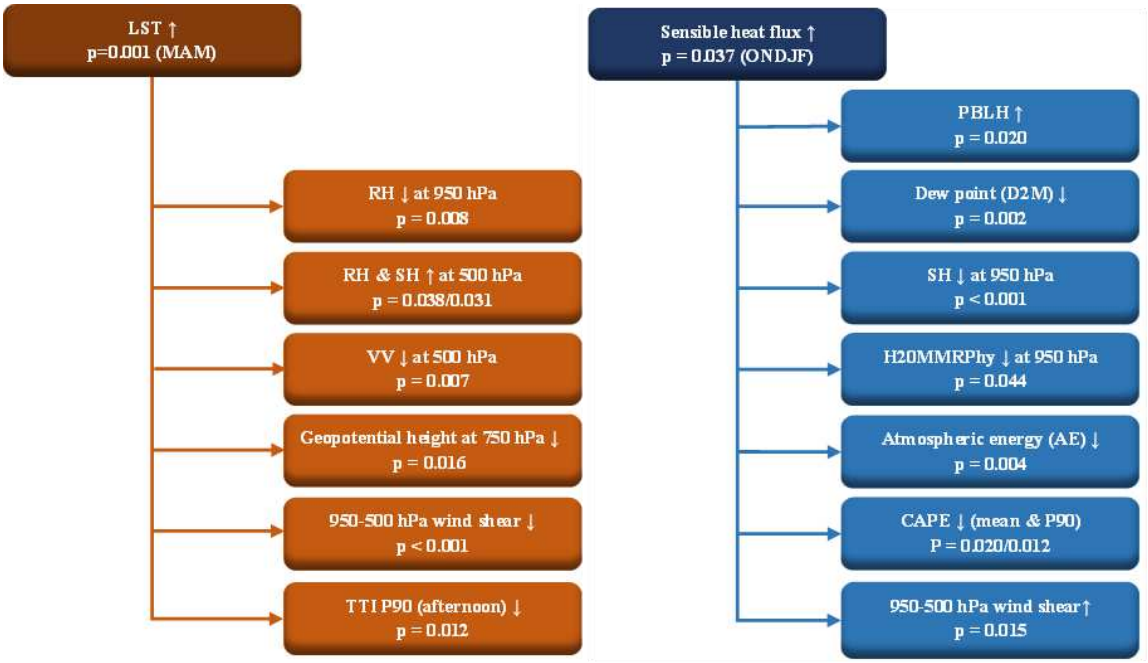


FIGURE IX. Schematic summary of the proposed seasonal thermodynamic evolution over Bhubaneswar (MAM and ONDJF)

Acknowledgment

The authors acknowledge the MOSDAC, ISRO, for providing INSAT-3D and INSAT-3DR satellite data, and ECMWF for providing ERA5 single level, ERA5 pressure level, and ERA5-Land reanalysis datasets used in the work.

Declaration

There is no funding received for this research.

References

1. Qian, Y., Chakraborty, T. C., Li, J., Li, D., He, C., Sarangi, C., ... & Leung, L. R. (2022). Urbanization impact on regional climate and extreme weather: Current understanding, uncertainties, and future research directions. *Advances in Atmospheric Sciences*, *39*(6), 819-860.
2. Long, H., Kong, X., Hu, S., & Li, Y. (2021). Land Use Transitions under Rapid Urbanization.
3. Grimmond, S. U. E. (2007). Urbanization and global environmental change: local effects of urban warming. *The Geographical Journal*, *173*(1), 83-88.
4. Maheng, D., Pathirana, A., Bhattacharya, B., Zevenbergen, C., Lauwaet, D., Siswanto, S., & Suwondo, A. (2024). Impact of land use land cover changes on urban temperature in Jakarta: insights from an urban boundary layer climate model. *Frontiers in Environmental Science*, *12*, 1399041.
5. Arnfield, A. J. (2003). Two decades of urban climate research: a review of turbulence, exchanges of energy and water, and the urban heat island. *International Journal of Climatology: a Journal of the Royal Meteorological Society*, *23*(1), 1-26.
6. Oke, T. R. (1982). The energetic basis of the urban heat island. *Quarterly journal of the royal meteorological society*, *108*(455), 1-24.
7. Xin, J., Zhang, Y., Bai, W., & Song, Z. (2024). Response of urban heat island effects within the planetary boundary layer to heat waves and impact of horizontal advection over Shanghai. *Atmospheric Research*, *311*, 107721.
8. Zhuang, Q., Koukoula, M., Liu, S., Zhou, Z., Gao, L., & Peleg, N. (2024). Contradictory influences of urbanization on intense convective rainfall in a subtropical city. *Environmental Research Letters*, *19*(10), 104020.
9. Chiu, C. T., Wang, K., Paschalis, A., Erfani, T., Peleg, N., Fatichi, S., ... & Manoli, G. (2022). An analytical approximation of urban heat and dry islands and their impact on convection triggering. *Urban Climate*, *46*, 101346.
10. Anasuya, B., Swain, D., & Vinoj, V. (2019). Rapid urbanization and associated impacts on land surface temperature changes over Bhubaneswar Urban District, India. *Environmental Monitoring and Assessment*, *191*(Suppl 3), 790.
11. Panigrahi, M., & Sharma, A. (2025). Urban growth dynamics and its influence on land surface temperature in Bhubaneswar metropolitan city: a 1990–2021 analysis. *Discover Applied Sciences*, *7*(2), 118.
12. Nayak, H. P., Nandini, G., Vinoj, V., Landu, K., Swain, D., Mohanty, U. C., & Niyogi, D. (2023). Influence of urbanization on winter surface temperatures in a topographically asymmetric Tropical City, Bhubaneswar, India. *Computational Urban Science*, *3*(1), 36.
13. Sethi, S. S., & Vinoj, V. (2024). Urbanization and regional climate change-linked warming of Indian cities. *Nature Cities*, *1*(6), 402-405.
14. Giri, R. K., Prakash, S., Yadav, R., & Saikrishnan, K. C. (2023). INSAT geostationary meteorological satellite program and current meteorological data processing system for INSAT-3D/3DR/3DS at India Meteorological Department. *Vayumandal*, *49*(1), 11-28.
15. Holton, J. R., & Hakim, G. J. (2013). *An introduction to dynamic meteorology* (Vol. 88). Academic press.
16. Yanai, M., Esbensen, S., & Chu, J. H. (1973). Determination of bulk properties of tropical cloud clusters from large-scale heat and moisture budgets. *Journal of Atmospheric Sciences*, *30*(4), 611-627.
17. Franzke, C. L., & Harnik, N. (2023). Long-term trends of the atmospheric circulation and moist static energy budget in the JRA-55 reanalysis. *Journal of Climate*, *36*(9), 2959-2984.

18. Minobe, S., Behrens, E., Findell, K. L., Loeb, N. G., Meyssignac, B., & Sutton, R. (2025). Global and regional drivers for exceptional climate extremes in 2023-2024: beyond the new normal. *NPJ climate and atmospheric science*, *8*(1), 138.
19. Muñoz-Sabater, J., Dutra, E., Agustí-Panareda, A., Albergel, C., Arduini, G., Balsamo, G., ... & Thépaut, J. N. (2021). ERA5-Land: A state-of-the-art global reanalysis dataset for land applications. *Earth system science data*, *13*(9), 4349-4383.
20. Hersbach, H., Bell, B., Berrisford, P., Hirahara, S., Horányi, A., Muñoz-Sabater, J., ... & Thépaut, J. N. (2020). The ERA5 global reanalysis. *Quarterly journal of the royal meteorological society*, *146*(730), 1999-2049.
21. Raj, B., Sahoo, S., Puviarasan, N., & Chandrasekar, V. (2025). Diurnal Analysis of Nor'westers over Gangetic West Bengal as Observed from Weather Radar. *Atmosphere*, *16*(8), 989.
22. Hamed, K. H., & Rao, A. R. (1998). A modified Mann-Kendall trend test for autocorrelated data. *Journal of hydrology*, *204*(1-4), 182-196.
23. Theil, H. (1992). A rank-invariant method of linear and polynomial regression analysis. In *Henri Theil's contributions to economics and econometrics: Econometric theory and methodology* (pp. 345-381). Dordrecht: Springer Netherlands.
24. Sen, P. K. (1968). Estimates of the regression coefficient based on Kendall's tau. *Journal of the American statistical association*, *63*(324), 1379-1389.
25. Cui, W., Galarneau Jr, T. J., & Hoogewind, K. A. (2024). Changes in mesoscale convective system precipitation structures in response to a warming climate. *Journal of Geophysical Research: Atmospheres*, *129*(9), e2023JD039920.
26. Ray, A., Chakraborty, T., Radhakrishnan, A., Hens, C., Dana, S. K., Ghosh, D., & Murukesh, N. (2023). Pattern change of precipitation extremes in Bear Island. *arXiv preprint arXiv:2312.04502*.
27. Beniston, M., & Stephenson, D. B. (2004). Extreme climatic events and their evolution under changing climatic conditions. *Global and planetary change*, *44*(1-4), 1-9.
28. Ferro, C. A., Hannachi, A., & Stephenson, D. B. (2005). Simple nonparametric techniques for exploring changing probability distributions of weather. *Journal of Climate*, *18*(21), 4344-4354.
29. Davis, I., Li, F., & Chavas, D. R. (2024). Future changes in the vertical structure of severe convective storm environments over the US central Great Plains. *Journal of Climate*, *37*(21), 5561-5578.
30. Weisman, M. L., & Klemp, J. B. (1982). The dependence of numerically simulated convective storms on vertical wind shear and buoyancy. *Monthly Weather Review*, *110*(6), 504-520.
31. Lanzante, J. R. (1996). Lag relationships involving tropical sea surface temperatures. *Journal of Climate*, *9*(10), 2568-2578.
32. Runge, J., Petoukhov, V., & Kurths, J. (2014). Quantifying the strength and delay of climatic interactions: The ambiguities of cross correlation and a novel measure based on graphical models. *Journal of climate*, *27*(2), 720-739.
33. Saragih, Y. F. (2023). Accuracy of the Moving Averages and Deseasonalizing Methods for Trend, Cyclical and Seasonal Data Forecasting. *JMEA: Journal of Mathematics Education and Application*, *2*(3), 143-151.
34. Krishnaveni, R B., Satapathy J., Jangid B.P, (2026) Cloud radiative effects over Indian regional atmosphere using CERES observations and machine learning regressions. *Atmospheric Research, 2*, (332), 108705.